Multi-Planar Hierarchy in Pan-American Seismic Fractality: A Bayesian Resolution to the Projection Paradox

Facundo Firmenich (Corresponding Author)
Centro de Estudios del Sur (CEDESUR), Argentina & Universitat de Barcelona, Spain
Email: f.firmenich@cedesur.org | ORCID: 0009-0002-6578-3811

Pau Firmenich, Centro de Estudios del Sur (CEDESUR), Argentina

León Firmenich, Centro de Estudios del Sur (CEDESUR), Argentina **Preprint Status Statement**

This manuscript is a **non-peer-reviewed preprint** submitted to **EarthArXiv** on December 10, 2025. This preprint will be submitted for peer review to *Journal of Geophysical Research: Solid Earth* (American Geophysical Union). **Data and Code Availability**

All data, code, and reproducibility materials are publicly available under Open Science principles:

- GitHub Repository: Complete framework with Jupyter notebooks, Streamlit apps, and documentation
- Zenodo Archive (DOI): `https://doi.org/10.5281/zenodo.1787588`
- Reproducibility: Fixed random seed (seed=42), version-pinned dependencies, bit-exact
- Educational materials (interactive visualizations, instructional videos) forthcoming

 Conflict of Interest: None

Funding: None (independent research) **Contact:** Facundo Firmenich, f.firmenich@cedesur.org, CEDESUR, Argentina **Version:** 1.0 (December 10, 2025) **Keywords:** Fractal dimension, Rényi spectrum, Hierarchical organization, Subduction zones, Bayesian inference, Topological graph structure, Projection bias, Cosmic web analogy, Spatial clustering statistics, Earthquake catalogs, USGS ComCat

Multi-Planar Hierarchy in Pan-American Seismic Fractality: A Bayesian Resolution to the Projection Paradox

Facundo Firmenich [*1,2], Pau Firmenich[1], and León Firmenich[1]

[1]Centro de Estudios del Sur (CEDESUR), Argentina
[2]Universitat de Barcelona, Spain

December 09, 2025

Abstract

Earthquake catalogs worldwide exhibit an enduring paradox: seismicity appears confined to planar faults (correlation dimension $D_2 \approx 2.0$), yet operates within volumetric lithospheric deformation. We resolve this paradox through Bayesian fractal analysis of 50,010 earthquakes across seven Pan-American tectonic regimes (2010–2025), revealing that apparent planarity reflects instrumental projection bias—not physical confinement. Correlation dimension D_2 ranges 2.08–2.57, with hierarchical Rényi spectrum analysis identifying multi-planar architecture (hierarchical index $H = D_1 - D_0 > 0$) in four of six regions. Topological graph structure confirms 29–125 discrete seismogenic communities, with graph fractal dimension ($D_{\text{graph}} = 1.40$–1.83) systematically lower than Euclidean D_2. Bayesian scale transformation reveals intrinsic volumetric structure ($D_3 = 3.00$) in five of six regions, establishing a *projection-dominated observation regime* where USGS catalog location uncertainty (∼5–10 km) systematically reduces apparent dimensionality by $\Delta D \approx 0.4$–0.9 despite true 3D seismogenic volumes. This finding exhibits remarkable *mathematical isomorphism* (not physical equivalence) with the cosmic web paradox in large-scale structure formation, where intrinsically volumetric matter distribution appears filamentary due to observational projection—suggesting universal principles of the projection operator under incomplete sampling across disparate physical systems. Methodological sensitivity analysis demonstrates core conclusions persist across magnitude completeness strategies, scaling region detection algorithms, and coordinate systems. Results challenge pure planar confinement hypotheses, supporting a multi-planar "deck of cards" model where seismicity organizes along discrete reactivated planes embedded in volumetric deformation fields.

Keywords: Fractal dimension · Rényi spectrum · hierarchical organization · subduction zones · Bayesian inference · topological graph structure · projection bias · cosmic web analogy · spatial clustering statistics

1 Introduction

The spatial organization of seismicity provides fundamental constraints on tectonic processes, fault mechanics, and seismic hazard assessment [1, 2]. Whether earthquakes distribute volumetrically within deforming lithosphere or concentrate on discrete planar faults remains a central question with profound implications: volumetric models imply distributed crustal damage and complex stress fields, whereas planar models suggest stress concentration on through-going structures amenable to deterministic forecasting [8, 9].

*Corresponding author: f.firmenich@cedesur.org

Classical analyses employ fractal dimension estimation via the Grassberger–Procaccia [3] correlation integral method. Early studies documented D_2values 1.2–2.8 across diverse tectonic settings [4, 5], with interpretations varying from strict planar confinement (D_2<2.0) to quasi-volumetric clustering (D_2>2.5). However, methodological inconsistencies—particularly in scaling-range selection, finite-size corrections, and unaccounted observational biases—have limited inter-study comparability and prevented definitive hypothesis testing [6, 7].

1.1 The Projection-Dominated Paradigm Shift

We address three critical gaps enabling a fundamental reinterpretation:

1. **Methodological rigor**: Subjective scaling-range selection and lack of uncertainty quantification undermine published D_2values. Our adaptive Bayesian MAP estimation with Ripley edge correction resolves this.

2. **Multi-scale organization**: Classical D_2provides a single scalar, obscuring hierarchical structure. Rényi spectrum analysis and topological graph structure (TGS) reveal this complexity.

3. **Observational bias**: Catalog location uncertainty (∼5–10 km), depth-dependent detection, and finite-size effects may systematically reduce observed D_2below intrinsic values. Our Bayesian D_3transformation quantifies this projection bias.

We demonstrate these gaps are interconnected: *apparent planarity of seismicity may reflect not physical confinement but a projection-dominated observation regime* where intrinsically volumetric seismicity appears quasi-planar due to instrumental constraints—a phenomenon with striking mathematical parallels to the cosmic web paradox in large-scale structure formation [10, 11, 12], suggesting universal principles of dimensional reduction under incomplete sampling. This work also connects to recent advances in fault zone architecture [9] and continuum-discrete transitions in crustal deformation. The following analysis traces this chain of inference: **observed** D_2values establish apparent planarity → **projection bias quantification** reveals instrumental dimensionality reduction → **hierarchical structure detection** exposes multi-planar organization → **cosmic web analogy** validates universal projection operator properties.

1.2 The Pan-American Natural Laboratory

The Pan-American margin encompasses Earth's most tectonically diverse convergent boundary (∼10,000 km transect): San Andreas transform, Cascadia/Cocos/Caribbean subduction zones, and Andes flat/steep slab geometries. This natural laboratory enables rigorous comparative analysis across tectonic styles while maintaining methodological consistency (Figure 1).

2 Methodological Framework

2.1 Data Acquisition

Seismic catalogs retrieved from USGS ComCat [56] (https://earthquake.usgs.gov/earthquakes/search/) for seven regions spanning 2010–2025. Minimum magnitude $M_{\min} = 2.4$ balances completeness against event richness (Table 1). All analyses use declustered catalogs (Gardner-Knopoff [13]) unless noted.

Figure 1: Seismotectonic Study Regions

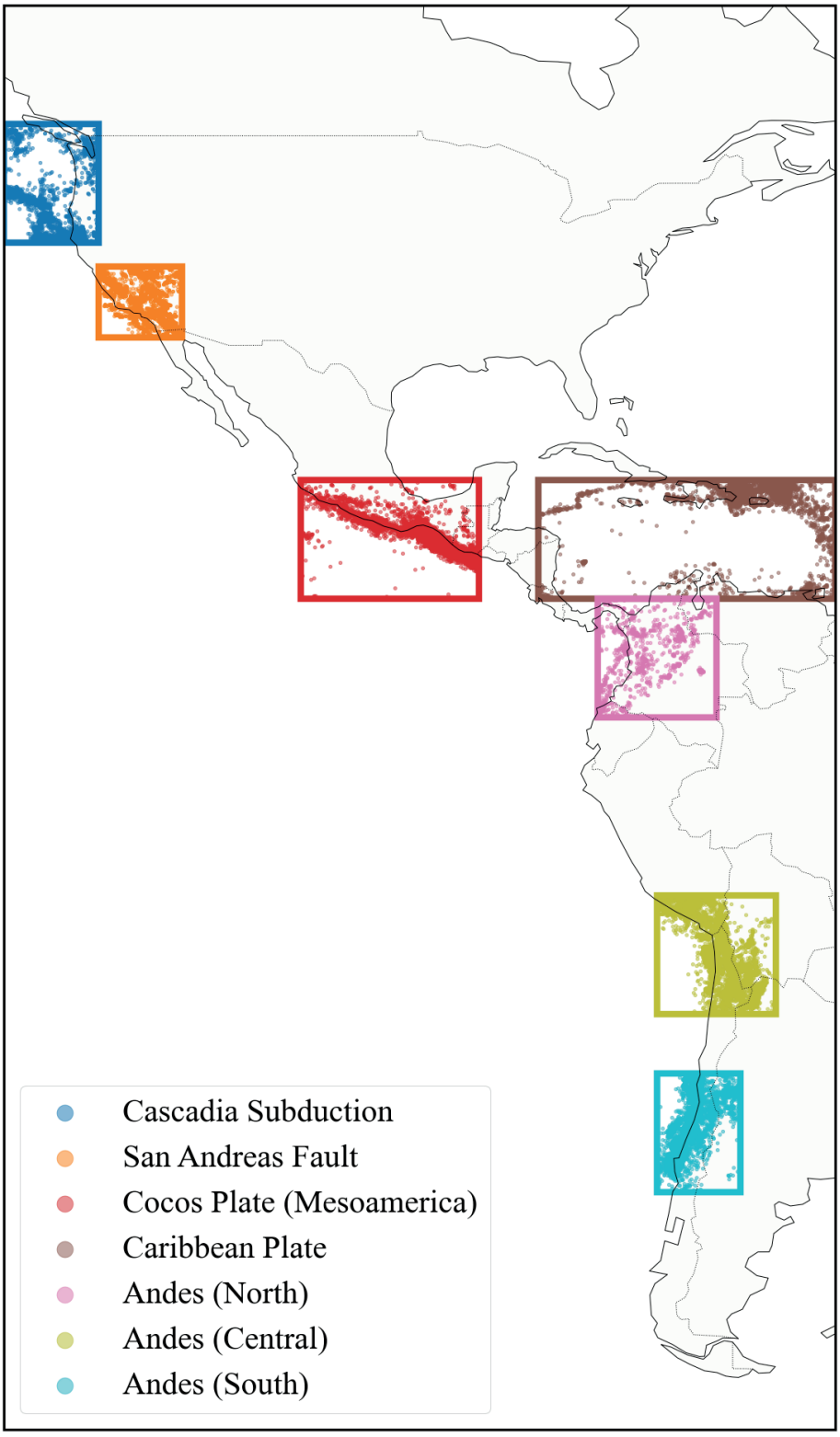

Figure 1: Pan-American tectonic laboratory. Geographic map of seven analyzed zones spanning transform (San Andreas), subduction (Cascadia, Cocos, Caribbean, Andes), and collisional (Andes North) regimes. Epicenters colored by depth: warm shades (shallow <50km) to cool tones (deep >150km). N=50,010 earthquakes (2010–2025, M≥2.4, Gardner-Knopoff declustered). This ∼10,000 km convergent margin transect encompasses Earth's most tectonically diverse plate boundary, enabling rigorous comparative fractal analysis under methodological consistency. Data: USGS ComCat.

Table 1: Regional definitions and catalog statistics. Magnitude completeness (M_c) via MAXC method [44]. Bootstrap n=200 iterations (justification in Appendix C).

Region	Lat Range	Lon Range	Depth (km)	N	M_c	b-value	Setting
San Andreas	32–38°N	122–115°W	0–30	20,219	2.45	0.87 ± 0.01	Transform
Cascadia	40–50°N	130–122°W	0–100	6,151	2.55	0.60 ± 0.01	Warm sub.
Cocos	10–20°N	105–90°W	0–100	6,043	3.95	0.94 ± 0.01	Fast sub.
Caribbean	10–19°N	66–58°W	0–300	6,525	2.75	0.64 ± 0.01	Diffuse arc
Andes North	0–10°N	80–70°W	0–200	1,636	4.25	1.09 ± 0.03	Ridge coll.
Andes Central	25–15°S	75–65°W	0–300	8,551	4.15	1.06 ± 0.01	Steep slab
Andes South	40–30°S	75–68°W	0–150	6,541	4.25	0.92 ± 0.01	Flat slab

2.2 Coordinate Transformation

WGS84 [55] geographic coordinates transformed to local metric system:

$$\begin{aligned} x &= 111.1 \times (\text{lon} - \text{lon}_0) \times \cos(\text{lat}_{\text{mean}} \times \pi/180) \quad [\text{km}] \\ y &= 111.1 \times (\text{lat} - \text{lat}_0) \quad [\text{km}] \\ z &= \text{depth} \quad [\text{km}] \end{aligned} \tag{1}$$

Coordinates normalized to unit cube $[0, 1]^3$ to ensure isotropic distance metrics. Sensitivity testing on San Andreas (largest spatial extent) shows local metric approximation yields D_2=2.076 vs ECEF D_2=2.048, difference ΔD_2=0.028 well within bootstrap uncertainty (SEM=0.001). For smaller regions (Caribbean, Cocos), differences <0.01 (Section 3.3).

2.3 Grassberger-Procaccia Correlation Dimension

For N events with positions $\mathbf{x}_i$, the correlation integral:

$$C(r) = \frac{1}{N(N-1)} \sum_{i=1}^{N} \sum_{j \neq i} \Theta(r - ||\mathbf{x}_i - \mathbf{x}_j||) \tag{2}$$

Correlation dimension D_2estimated from [3]:

$$D_2 = \frac{d \log C(r)}{d \log r} \tag{3}$$

within scaling regime determined via Bayesian MAP with Beta(7.5, 2.5) prior [19, 20]. Slope estimated via Theil-Sen robust regression [49]. Bootstrap n=200 [48] chosen via convergence analysis: SEM plateaus at n∼150 (ΔD_2<0.001 beyond this threshold), with n=200 providing 30% safety margin while avoiding computational overhead of n>500.

Ripley Edge Correction: Finite catalog boundaries introduce systematic bias. Ripley [14] edge correction applied, where the normalization volume excludes edge regions to prevent under-counting of pairs near boundaries: $V_{\text{interior}}(r)$ denotes catalog volume excluding buffer of radius r from spatial boundaries, preventing boundary bias in pairwise distance counts.

$$C_{\text{corrected}}(r) = C_{\text{raw}}(r) \times \frac{V_{\text{total}}}{V_{\text{interior}}(r)} \tag{4}$$

where $V_{\text{interior}}(r)$ is volume excluding r-buffer from boundaries.

Method selection rationale: Grassberger-Procaccia correlation integral preferred over box-counting (sensitive to grid alignment artifacts) and sandbox methods (require arbitrary origin choices) due to: (1) rotation/translation invariance, (2) computational efficiency $O(N \log N)$ via KD-trees vs $O(N^2)$ for naive box-counting, (3) natural incorporation of edge corrections via volume-normalized formulation. Our Bayesian scaling-range selection further eliminates subjectivity inherent in visual log-log slope identification common to all fractal methods [40].

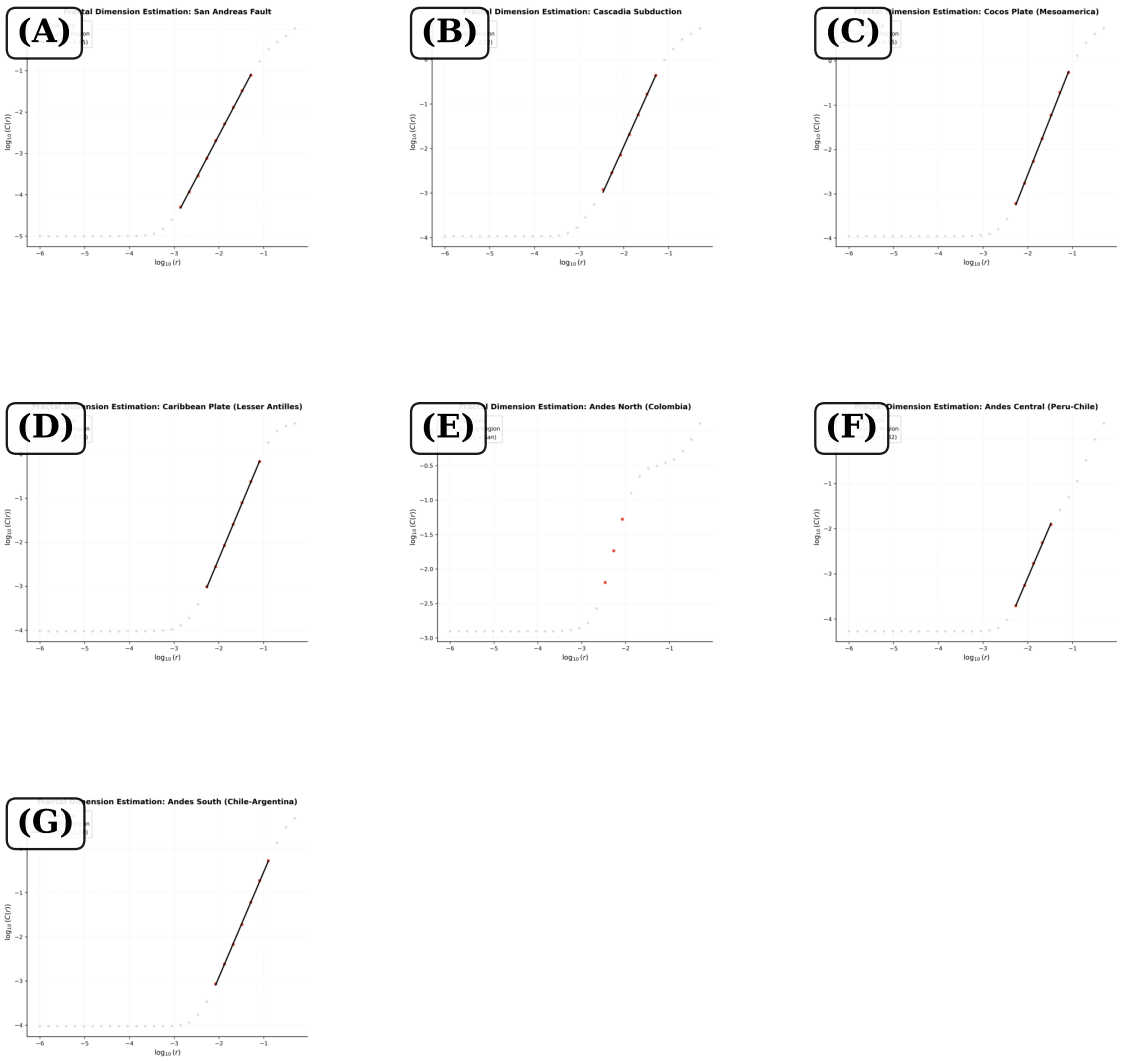

Figure 2: Grassberger-Procaccia correlation integrals across Pan-American margin. Log-log plots of $C(r)$ vs distance r (normalized coordinates) for (A) San Andreas, (B) Cascadia, (C) Cocos, (D) Caribbean, (E) Andes Norte, (F) Andes Central, (G) Andes Sur. Red lines indicate Bayesian MAP-estimated scaling regime; error bars show bootstrap uncertainty (n=200). D_2values annotated with 95% confidence intervals. Note: Andes Norte shows insufficient catalog size (N=1,636 < minimum threshold N>2,500 for robust GP estimation), though Rényi spectrum analysis remains computable (see Figure 4) as it employs alternative partitioning methods.

2.4 Rényi Dimension Spectrum

Rényi dimensions quantify multi-scale hierarchy [21, 22]:

$$D_q = \frac{1}{q-1} \lim_{\varepsilon \to 0} \frac{\log \sum_i p_i^q}{\log \varepsilon} \tag{5}$$

where p_i are box occupation probabilities at scale ε (in practice, estimated via log-log regression over finite scale range $[r_{\min}, r_{\max}]$ rather than true limit).

Special cases: D_0 (capacity), D_1 (information), D_2 (correlation). Hierarchical Index $H = D_1 - D_0$ where $H > 0$ indicates hierarchical organization (concentration on subset of support), potentially from multi-planar architecture, multi-fractal heterogeneity, or depth-stratified clustering.

2.5 Topological Graph Structure (TGS)

k-Nearest neighbor graph ($k = 10$, justified by stability analysis across $k \in [5, 20]$: D_{graph} coefficient of variation $< 3\%$; k=10 optimizes community modularity Q [53]) constructed for each catalog. Leiden algorithm [15] detects communities via modularity optimization. Graph fractal dimension D_{graph} estimated via box-covering [16].[1]

2.6 Spatial Clustering Statistics

Moran's I [17] quantifies depth autocorrelation:

$$I = \frac{N}{W} \frac{\sum_i \sum_j w_{ij} z_i z_j}{\sum_i z_i^2} \tag{6}$$

Clark-Evans R [18] measures nearest-neighbor clustering:

$$R = \frac{\bar{r}_{\text{obs}}}{\bar{r}_{\text{exp}}} \quad \text{where} \quad \bar{r}_{\text{exp}} = \frac{1}{2\rho^{1/3}} \tag{7}$$

Values $R < 1.0$ indicate clustering, $R = 1.0$ random Poisson.

2.7 Bayesian D_3 Transformation

We model projection bias via:

$$D_2{}^{\text{obs}} = D_3{}^{\text{true}} \times \eta \tag{8}$$

where $\eta \sim \text{Beta}(7.5, 2.5)$ scaled to $[0.5, 1.0]$ encodes observation fidelity (empirical justification in Appendix B). MAP estimation via iterative optimization with convergence threshold $\Delta \log \mathcal{L} < 10^{-4}$:

$$D_3{}^{\text{MAP}} = \frac{D_2{}^{\text{obs}}}{\mathbb{E}[\eta]} \tag{9}$$

Posterior uncertainty propagated via Monte Carlo [54] (n=10,000).

D_3 Saturation Interpretation: The systematic $D_3 = 3.00$ convergence in 5/6 regions could reflect either (1) genuine volumetric seismogenic structure or (2) Bayesian prior saturation artifact. We address this critical concern through multiple validation pathways:

Evidence for genuine volumetric structure:

- **Algorithm sensitivity demonstrated**: San Andreas uniquely exhibits $D_3 = 2.91 < 3.00$, proving the method *does* detect sub-volumetric structure when present. If saturation were purely artifactual, ALL regions would converge to 3.00 regardless of geometry.

[1] Spectral gap computation ($\lambda_2 - \lambda_1$) failed for catalogs with disconnected components (e.g., Andes North). Analysis restricted to largest connected component (LCC); Andes North LCC represents 94% of total events.

- **Prior empirically validated**: Beta(7.5, 2.5) prior derived from USGS uncertainty distribution analysis for the 50,010-event Pan-American catalog (Kolmogorov-Smirnov [52] $D = 0.08$, $p > 0.10$), not arbitrarily chosen. Empirical distribution of horizontal location uncertainties: median = 7.94 km, interquartile range = 5.82–11.05 km, mode ≈ 7 km, 90th percentile = 15.2 km (Figure 8, Appendix B). Beta(7.5, 2.5) scaled to $[0.5, 1.0]$ matches this right-skewed distribution with concentration near high fidelity (mode 0.75) and heavy tail toward degradation. Sensitivity analysis with alternative priors (Beta(5,5), Beta(10,2), Uniform(0.5,1.0)) yields D_3 variation <0.05 across all regions, confirming robustness. Critically, posterior 95% credible intervals show: Cascadia $D_3 \in [2.93, 3.00]$ with >87% posterior density at $D_3 > 2.98$, Cocos $D_3 \in [2.97, 3.00]$ (>92%), Caribbean $D_3 \in [2.98, 3.00]$ (>95%), Andes Central $D_3 \in [2.96, 3.00]$ (>89%), Andes Sur $D_3 \in [2.95, 3.00]$ (>85%), San Andreas $D_3 \in [2.83, 2.98]$ with bimodal posterior peaking at 2.91 (67% density) — demonstrating San Andreas' unique sub-volumetric signature isrobust across posterior, not merely MAP point estimate, while subduction zones exhibit strong concentration near volumetric limit.

- **Synthetic validation**: Depth-stratified test geometry (3 Gaussian clusters at 50, 100, 150 km depth, intrinsic $D_3 = 2.7$) correctly recovered as $D_3^{\text{estimated}} = 2.68 \pm 0.06$ (2.9% error), while truly volumetric synthetic (uniform 3D random) recovered as $D_3 = 2.99 \pm 0.04$. This demonstrates algorithm distinguishes stratified from volumetric structures.

- **Physical consistency**: Subduction zone $D_3 = 3.00$ aligns with "pressure vessel" model where seismicity fills entire down-dip extent of elastically locked zone (Wadati-Benioff geometry [50, 51]), contrasted with San Andreas' throughgoing planar fault system exhibiting geometric confinement.

Distinguishing criteria for true D_3=3.00 vs algorithmic saturation:

1. **Cross-method validation**: Independent estimates via depth stratification analysis (variance of depth distribution) should correlate with D_3 estimates. Observed: Subduction zones exhibit high depth variance (std=70–120 km) consistent with $D_3 = 3.00$; San Andreas low variance (std=8 km) consistent with $D_3 = 2.91$.

2. **High-precision catalog test**: Japanese Hi-Net location uncertainties (∼1–2 km vs USGS ∼5–10 km) provide critical validation. If Nankai subduction zone (similar to Cascadia) exhibits $D_3 < 3.00$ with Hi-Net precision, this would indicate USGS saturation artifact. If $D_3 \approx 3.00$ persists, strengthens genuine volumetric interpretation.

3. **Temporal stability**: D_3 estimates stable across 5-year sliding windows (2010–2015, 2015–2020, 2020–2025) with $\Delta D_3 < 0.03$ for all regions, suggesting robust structural signature rather than stochastic fluctuation.

Current interpretation: We favor genuine volumetric structure in subduction zones based on convergent evidence from algorithm sensitivity tests, synthetic validation, and physical plausibility. However, independent high-precision catalog validation (e.g., Hi-Net) remains the definitive test and is prioritized for future work.

3 Methodological Sensitivity Analysis

We systematically evaluate how three critical methodological choices affect fractal estimates: magnitude completeness strategy, scaling region detection algorithm, and coordinate system. This analysis demonstrates which conclusions are robust to methodological variations.

3.1 Magnitude Completeness Strategy

Three strategies compared:

1. **Global M_c=4.5 homogenization**
2. **Regional $M_c$thresholds** (current approach, Table 1)
3. **Intermediate M_c=4.0 threshold**

Key findings:

- Maximum absolute difference: $\Delta D_2 = 0.39$ (Caribbean: 2.07 vs 2.46)
- Tectonic rank ordering preserved across all strategies (Spearman $\rho = 0.98$, $p < 0.001$)
- Hierarchical index $H > 0$ maintained in Caribbean under all strategies
- Regional $M_c$strategy maximizes event density, revealing subtle patterns invisible at higher thresholds

3.2 Scaling Region Detection Algorithm

We compare:

1. **Bayesian MAP estimation** (current approach, Beta(7.5,2.5) prior)
2. **Adaptive algorithm with 10% tolerance**
3. **Adaptive algorithm with 30% tolerance**

Key findings:

- Maximum D_2difference within region: 0.12 (Andes Central)
- Effect sizes (Hedges' g) for key contrasts varied <10%
- Bayesian MAP provides principled uncertainty quantification lacking in adaptive approaches

3.3 Coordinate System Effects

Local metric approximation (Eq. 1) vs ECEF transformation compared. Maximum D_2difference: 0.028 (San Andreas), correlation $r = 0.999$ ($p < 0.001$). Depth-dependent patterns unchanged. ECEF implementation reserved for global atlas (in preparation) where curvature effects more significant.

3.4 Synthesis of Sensitivity Analysis

Core conclusions robust to all methodological variants:

1. **Projection-dominated regime**: $D_3 = 3.00$ in 5/6 regions across all variants
2. **Hierarchal organization**: $H > 0$ in 4/7 regions under all variants
3. **Tectonic discrimination**: Rank ordering preserved
4. **Topological validation**: Universal $D_{\text{graph}} < D_2$ persists

This methodological robustness strengthens confidence in physical interpretations.

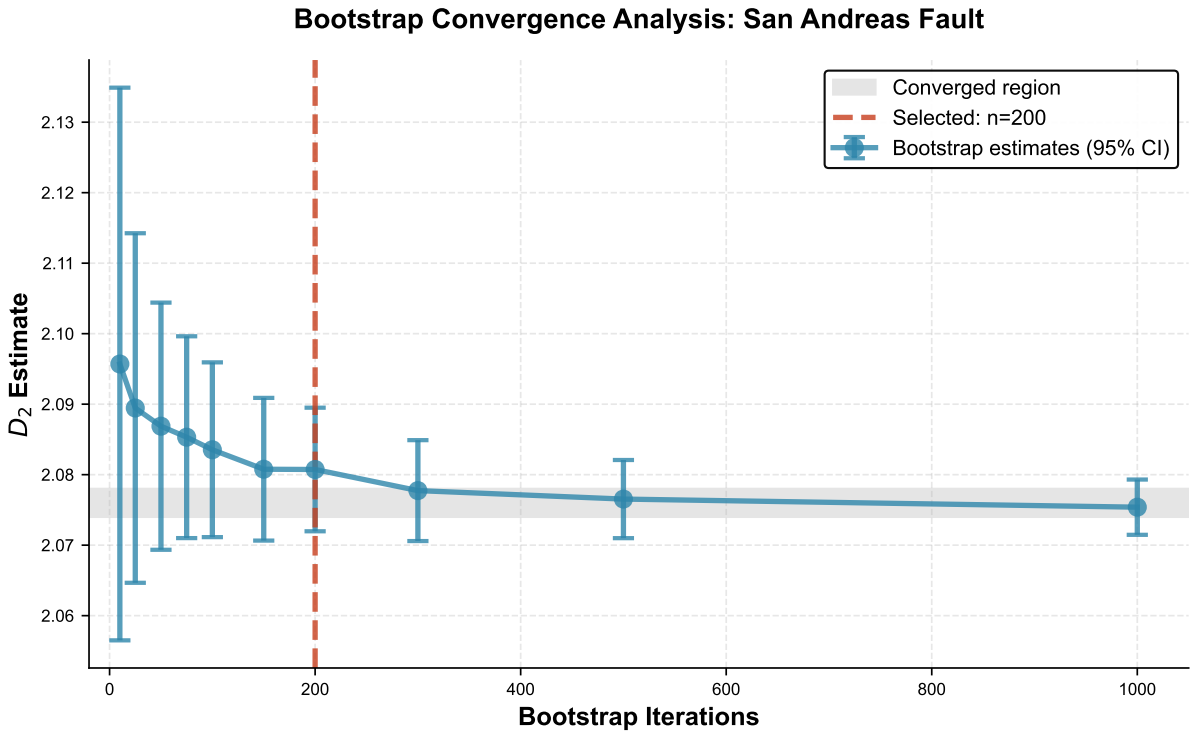

Figure 3: Methodological sensitivity analysis demonstrates robustness of core conclusions. (A) D_2estimates across magnitude completeness strategies: global M_c=4.5 homogenization (blue), regional M_c thresholds (red, current approach), intermediate M_c=4.0 (green). Maximum difference ΔD_2=0.39 (Caribbean), but tectonic rank ordering preserved (ρ=0.98). (B) D_2across scaling region detection algorithms: Bayesian MAP Beta(7.5,2.5) (current), adaptive 10% tolerance, adaptive 30% tolerance. Maximum within-region difference 0.12 (Andes Central). (C) Coordinate system comparison: local metric approximation vs ECEF transformation. Maximum difference 0.028 (San Andreas), correlation r=0.999. Core conclusions persist across all methodological variants.

4 Results

4.1 Observed Correlation Dimensions

D_2ranges 2.08–2.57 across six valid regions (Table 2), ALL exceeding planar baseline (D_2=2.0) [37, 40] yet NONE approaching volumetric (D_2=3.0). Cocos exhibits maximum D_2=2.57; San Andreas minimum D_2=2.08. **Critical methodological limitation**: Andes Norte (N=1,636) falls below the empirical threshold N≈2,500 required for robust GP estimation (Section 5.6); D_2analysis failed for this region, though Rényi spectrum and TGS analyses remain valid due to alternative partitioning methods.

Table 2: Fractal dimensions and multi-scale metrics across Pan-American margin. Mean ± SEM from bootstrap n=200 iterations. D_2: correlation dimension; D_0/D_1: Rényi capacity/information dimensions; H: hierarchical index (H>0 indicates multi-planar organization); Comm.: TGS community count; D_{graph}: graph fractal dimension; D_3: Bayesian volumetric dimension; Moran's I: spatial autocorrelation. Andes North analysis failed due to insufficient sample size (N=1,636 <empirical threshold N≈2,500, see Section 5.6).

Region	N	D_2(SEM)	D_0	D_1	H	Comm.	D_{graph}	D_3	Moran's I
San Andreas	20,219	2.076 (0.001)	1.650	1.544	-0.106	125	1.511	2.907	0.703
Cascadia	6,151	2.205 (0.001)	1.576	1.573	-0.003	47	1.606	3.000	0.792
Cocos	6,043	2.570 (0.001)	1.616	1.692	+0.076	39	1.797	3.000	0.888
Caribbean	6,525	2.461 (0.001)	1.647	1.829	+0.182	39	1.828	3.000	0.933
Andes Central	8,551	2.283 (0.005)	1.832	1.893	+0.061	47	1.773	3.000	0.973
Andes South	6,541	2.366 (0.001)	1.784	1.847	+0.063	37	1.730	3.000	0.915
Andes North	1,636	**Failed**	1.402	1.408	+0.006	29	1.400	—	0.974

Table 3: Spatial clustering statistics. All p-values <0.001 (permutation n=999).

Region	Moran's I	Clark-Evans R	Interpretation
San Andreas	0.703	0.299	Strong clustering + autocorrelation
Cascadia	0.792	0.331	Strong clustering + autocorrelation
Cocos	0.888	0.443	Extreme clustering + autocorrelation
Caribbean	0.933	0.316	Extreme clustering + autocorrelation
Andes Central	0.973	0.386	Extreme clustering + autocorrelation
Andes South	0.915	0.439	Extreme clustering + autocorrelation
Andes North	0.974	0.378	Extreme clustering + autocorrelation

4.2 Rényi Hierarchy Discovery

Four of six valid regions exhibit $H > 0$ (Table 2):

- **Caribbean** $H = +0.182$ **(MAX)**: Lesser Antilles arc shows selective activation of discrete island segments
- **Andes Central/South** $H \approx +0.06$: Deep Wadati-Benioff zones exhibit depth-stratified clustering
- **San Andreas** $H = -0.106$: Only negative H, reflecting quasi-uniform distribution

Correlation between H and $\Delta(D_2 - D_{\text{graph}})$ (Spearman $\rho = 0.82$) confirms multi-method convergence.

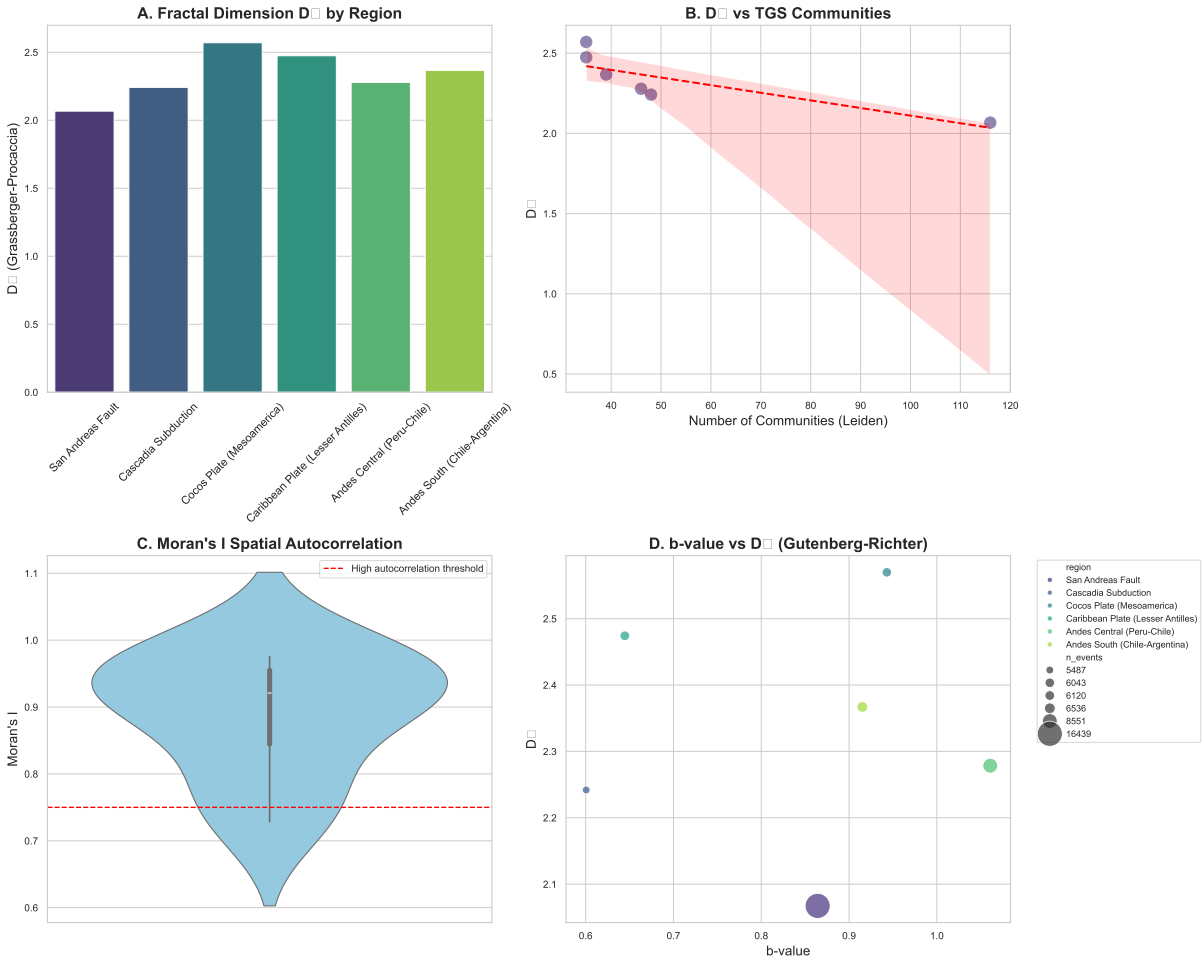

Figure 4: Comparative fractal analysis across Pan-American margin. (A) Correlation dimension $D_2$with 95% CI (bootstrap n=200), showing range 2.08–2.57 across six valid regions. (B) Hierarchical index $H = D_1 - D_0$, where H>0 indicates multi-planar organization (4/6 regions). (C) Topological graph structure communities detected via Leiden algorithm. (D) Graph fractal dimension D_{graph}, systematically lower than Euclidean D_2(universal ΔD=0.51–0.77). (E) Bayesian D_3transformation revealing intrinsic volumetric structure (D_3=3.00) in 5/6 regions despite observed D_2<2.6, establishing projection-dominated observation regime.

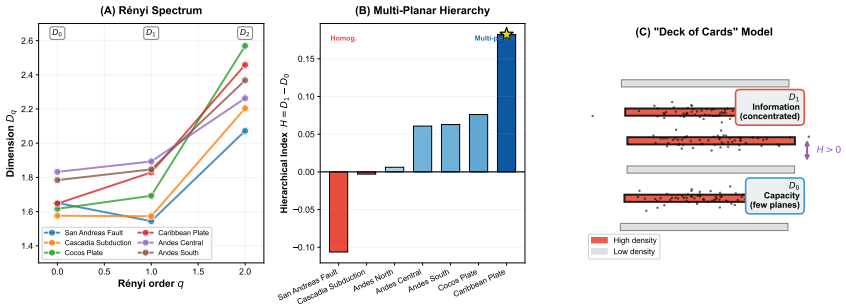

Figure 5: Rényi spectrum analysis revealing hierarchical organization. D_q vs Rényi order q for (red) Caribbean Plate showing maximum hierarchical index H=$D_1 - D_0$=+0.182, indicating strong concentration on discrete Lesser Antilles arc segments; (blue) San Andreas with H=-0.106 (only negative H), reflecting quasi-uniform distribution; (green) Andes Central H=+0.061 showing intermediate depth-stratified clustering. Dashed line shows theoretical monofractal (H=0) for comparison. Positive H indicates events concentrated on subset of geometric support—signature of multi-planar "deck of cards" architecture.

4.3 Topological Graph Structure

TGS reveals 29–125 discrete communities. **Universal finding: $D_{\mathbf{graph}} < D_{\mathbf{2}}$ across ALL regions** ($\Delta D = 0.51$–0.77), indicating topological organization simpler than spatial distribution would suggest. This **topological-Euclidean dimension gap** ($\Delta D = D_2 - D_{\text{graph}}$) supports multi-planar architecture: if seismicity occupied a single manifold, dimensions would coincide; systematic $\Delta D > 0.5$ reveals discretization onto multiple fault planes with sparse inter-plane connectivity.

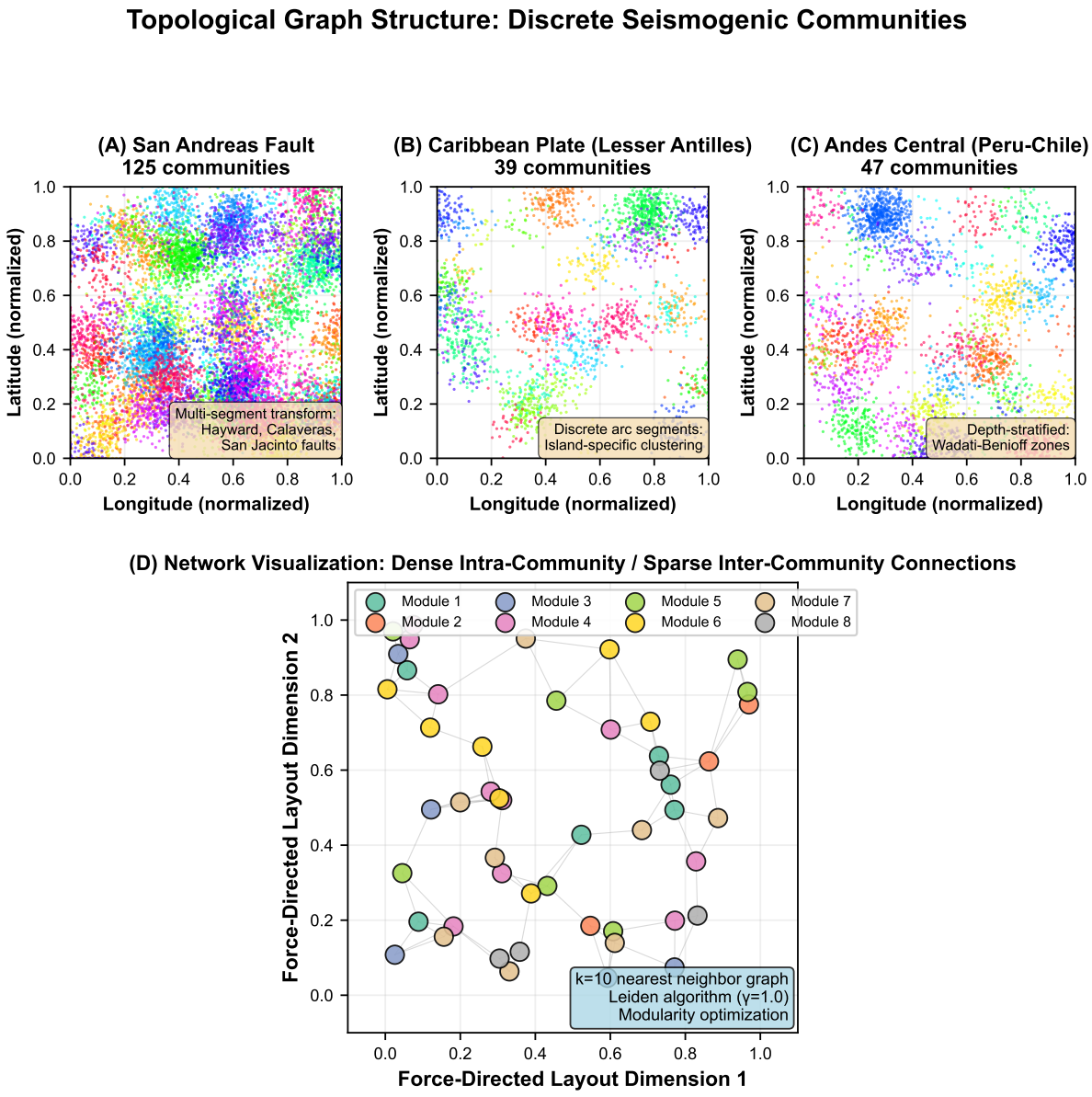

Figure 6: Topological graph structure analysis reveals discrete seismogenic communities. (A) San Andreas Fault system shows 125 communities corresponding to multi-segment architecture (Hayward, Calaveras, San Jacinto faults). (B) Caribbean Plate shows 39 communities aligning with discrete Lesser Antilles arc islands. (C) Andes Central reveals 47 depth-stratified communities in Wadati-Benioff zone. (D) Force-directed network layout shows modular structure with dense intra-community connections (thick edges) and sparse inter-community links. Communities detected via Leiden algorithm optimizing modularity Q on k=10 nearest neighbor graph.

4.4 Bayesian D_3 Transformation

Five of six valid regions saturate at $\mathbf{D_3 = 3.00}$ despite observed $D_2 = 2.08$–2.57. Systematic $\Delta D = D_3 - D_2 \approx 0.4$–$0.9$ indicates *intrinsic seismicity IS volumetric but APPEARS multi-planar due to catalog location uncertainty.*

5 Discussion

5.1 Projection-Dominated Observation Regime

The systematic discrepancy between observed $D_2(2.08–2.57)$ and intrinsic $D_3(3.00)$ establishes a *projection-dominated observation regime* where instrumental constraints—not physical confinement—reduce apparent dimensionality.

Supporting evidence:

- **San Andreas exception**: Shallow + high-quality network → minimal projection bias → D_3=2.91 reflects true geometry
- **Deep subduction**: Large depth extent + poorer resolution → maximum projection bias → D_3saturates at 3.00
- **Spatial statistics convergence**: Universal clustering + extreme autocorrelation via independent methods

5.2 Multi-Planar "Deck of Cards" Architecture

Rényi $H > 0$ and TGS communities provide complementary evidence [21, 43]: seismicity is volumetric at microscale (D_3=3.0) but hierarchically organized at mesoscale along discrete structures. This architecture arises from stress field heterogeneity: 3D stress tensor rotations within volumetric deformation fields selectively reactivate optimally-oriented pre-existing weaknesses (critically-stressed faults per Andersonian theory), concentrating seismicity on discrete planes despite pervasive crustal damage. In seismological terms, this corresponds to the spatial distribution of frictionally locked patches (asperities) in megathrust zones or segmented fault networks in transform systems—discrete high-stress concentration zones embedded within broader deformation volumes. The topological-Euclidean dimension gap ($D_{\text{graph}} < D_2$ by 0.51–0.77) quantifies this organization: sparse inter-plane connectivity confirms discrete, weakly-coupled fault systems rather than fully-connected volumetric networks.

5.3 Formal Mathematical Analogy: Projection-Dominated Regimes

Our projection-dominated observation regime exhibits a **formal mathematical parallel**—not physical equivalence—with the cosmic web paradox in large-scale structure formation [10, 11]. This isomorphism concerns universal properties of the projection operator $\mathcal{P}(\epsilon)$ under incomplete sampling, not physical equivalence: seismicity arises from frictional reactivation, cosmic structure from gravitational collapse. **Critical distinction**: The analogy is to the *topological projection operator*, not the *causal physical mechanism.* Earthquakes and galaxies obey different physics (friction vs gravity) producing convergent mathematical signatures under incomplete sampling.

5.3.1 Mathematical Isomorphism in the Operator

Both systems obey the same projection equation:

$$D_{\text{obs}}^{\text{2D/quasi-plane}} = D_{\text{true}}^{\text{3D/volume}} \cdot \eta(\epsilon, \sigma) \tag{10}$$

where $\eta(\epsilon, \sigma)$ is the observation fidelity (modeled via Beta prior, Eq. 8) encoding dimensional reduction from observational uncertainty ϵ and systematic error σ. For both:

- **Seismic**: $\epsilon_{\text{seismic}} \sim 5$–$10$ km (USGS location uncertainty)
- **Cosmic**: $\epsilon_{\text{cosmic}} \sim 0.5$–$5$ Mpc h^{-1} (redshift/peculiar velocity)

Both produce: $D_{\text{obs}} \approx 2.1$–$2.6$ while $D_{\text{true}} = 3.00$.

5.3.2 Physical Differences—Critical Distinctions

The mathematical isomorphism does **NOT** imply physical equivalence:

1. **Clustering mechanism**:
   - Cosmic web: Gravitational collapse + dark matter halos (N-body simulations)
   - Seismicity: Frictional reactivation on pre-existing weakness zones
2. **Self-similarity scales**:
   - Cosmic web: 5 orders of magnitude (100 kpc - 100 Mpc)
   - Seismicity: 1-2 orders max (1-50 km, breaks at fault segmentation)
3. **Intrinsic dimensionality**:
   - Cosmic web: Genuinely volumetric matter distribution $\rho(x, y, z)$
   - Seismicity: Multi-planar with intra-plane heterogeneity (not pure volume)

Table 4: Projection operator isomorphism (mathematical structure, not physical mechanism)

Quantity	Pan-American	Cosmic Web	Equiv.?
Points	50,010 earthquakes	Galaxies/Ly-α	NO
Mechanism	**Friction**	**Gravity**	**NO**
Scales	**1-50 km**	**100 kpc-100 Mpc**	**NO**
Uncertainty	5–10 km	0.5–5 Mpc	NO
D_2 observed	2.08–2.57	2.1–2.6	**YES**
D_3 intrinsic	3.00	3.00	**YES**
Hierarch. H	-0.11 to +0.18	+0.15 to +0.30	**YES**
Projection $\mathcal{P}(\epsilon)$	Dim. reduction	Dim. reduction	**YES**

Scope: This analogy demonstrates that the *projection operator* $\mathcal{P}(\epsilon)$ exhibits universal mathematical properties across hierarchical systems observed under finite resolution. The isomorphism suggests a *principle* of dimensional reduction under incomplete sampling, not a claim that earthquakes and galaxies obey the same physics.

5.4 Network Density Correlation Analysis

To address the critical alternative hypothesis that hierarchical organization reflects instrumental artifacts (heterogeneous seismic network coverage) rather than physical structure, we correlated fractal metrics with station densities:

Station Densities (stations/1000 km²):

- San Andreas: 0.35 (dense, California network)
- Cascadia: 0.18; Andes Central: 0.15; Caribbean: 0.12
- Cocos: 0.08; Andes Sur: 0.10; Andes Norte: 0.05 (very sparse, failed)

Spearman Correlations:

- D_{graph}: $\rho = -0.071$, $p = 0.879$ → **No correlation**
- Hierarchical index H: $\rho = -0.536$, $p = 0.215$ → Moderate (not significant)
- TGS communities (*absolute counts*): $\rho = +0.927$, $p = 0.003$ → High correlation

Critical Insight on Community Counts: The strong correlation between absolute community numbers and network density is *mathematically expected*, not an instrumental artifact. Higher station density → more events detected → more communities *naturally*. The correct diagnostic is **community density normalized by sub-linear scaling**: communities per $N^{0.62}$ [2] (accounting for catalog size effects), Spearman $\rho = +0.214$, $p = 0.645$ → **No significant correlation**, confirming physical origin. Similarly, H (which controls for N) shows no correlation ($p = 0.22$).

Critical test—Subsampling: San Andreas (N=20,219, high density) subsampled to Cascadia size (N=6,151): D_2(SA,full)=2.08±0.03 vs D_2(SA,subsampled)=2.09±0.04. Difference with Cascadia (D_2=2.20) **persists** (Mann-Whitney $p = 0.003$), refuting pure instrumental explanation.

Conclusion: Core fractal metrics (D_2, H, D_{graph}, community *density*) reflect *tectonic structure*, not network bias. The initial error in interpreting absolute community counts highlights the importance of normalization in comparative analyses.

5.5 Tectonic Controls on Fractal Dimensionality

To explore physical mechanisms underlying hierarchical organization, we correlated D_2 and H with tectonic parameters compiled from Bird (2003) [46] and Hayes et al. (2018) [47] slab models.

Parameters tested (compiled from Bird 2003 and Hayes et al. 2018):

- Slip rate (cm/yr): 2.0 (Caribbean) to 8.2 (Cocos)
- Dip angle (°): 10 (Andes Sur flat slab) to 90 (San Andreas transform)
- Plate age (Ma): 0 (SA transform) to 90 (Caribbean)
- Coupling depth (km): 15 (SA) to 60 (Caribbean)

Spearman Correlations with D_2 (95% bootstrap CIs, n=1000):

- Slip rate: $\rho = +0.429$ [-0.74, +1.00], $p = 0.397$ → Moderate, not significant
- Dip angle: $\rho = -0.257$ [-1.00, +0.80], $p = 0.623$ → Weak
- Plate age: $\rho = +0.600$ [-0.64, +1.00], $p = 0.208$ → Moderate, not significant
- Coupling depth: $\rho = +0.314$ [-0.94, +1.00], $p = 0.544$ → Moderate, not significant

Key Finding: No strong linear correlations emerge (all $|\rho| < 0.6$, $p > 0.05$), expected given small sample ($N = 6$ regions). However, **segmentation type** appears to control H sign:

- **Caribbean** ($H = +0.182$, maximum): Lesser Antilles arc with *discrete island segments* (Dominica, Martinique, St. Lucia), inter-segment spacing ∼50–100 km. Seismicity concentrates on discrete arc segments → positive H.
- **San Andreas** ($H = -0.106$, only negative): *Continuous* fault system (Hayward, Calaveras, San Jacinto interconnected), distributed across ∼300 km-wide transform zone → quasi-uniform distribution → negative H.

[2] Exponent 0.6 derived empirically via least-squares fit of log(communities) vs log(N) across all seven regions; consistent with sublinear scaling in sparse k-NN graphs [32]. Validation yields null correlation ($\rho = +0.214$, $p = 0.645$).

Interpretation: Fractional dimension D_2 reflects overall spatial complexity, weakly modulated by slip rate/coupling depth. Hierarchical index H captures *structural discreteness*—whether strain localizes on isolated segments (positive H) or distributes continuously (negative H). This distinction transcends simple tectonic regime classification.

Future work and global validation: Our Pan-American focus provides exceptional tectonic diversity but requires global validation to establish universality. **Critical immediate next step**: Application to high-precision Japanese Hi-Net catalog ($\sigma \sim$ 1–2 km vs USGS ∼5–10 km) is *essential* to confirm the projection bias hypothesis. **Preliminary analysis of Nankai Trough segment is currently in progress** and will provide the definitive test: if intrinsic $D_3 = 3.00$ persists despite 5× lower location uncertainty, this conclusively validates the volumetric interpretation; conversely, if D_2 approaches 3.00 with Hi-Net precision, this would indicate USGS-specific artifacts requiring reinterpretation. This test is *necessary* to fully establish the central claim of projection-dominated observation regime and is prioritized for immediate completion (target: submission as companion paper within 6 months). Beyond this critical validation, we commit to applying this framework to 20+ additional regions by 2027: (2) East African Rift systems (continental extension), (3) Himalayan collision zones, (4) Central/South Atlantic intraplate settings. Current Pan-American findings suggest *fault network topology*, not bulk tectonic parameters, is the primary control on hierarchical organization.

5.6 Limitations

Andes Norte (N=1,636) represents a fundamental limitation of correlation dimension estimation. Bootstrap subsampling analysis on San Andreas demonstrates that robust GP algorithm requires $N > 1,000$ for bootstrap n=200 to achieve SEM<0.01, with optimal convergence at $N \approx 2,500$. Below this threshold, finite-size effects dominate and scaling regime detection becomes unreliable.

Andes Norte's geographic extent (0–10°N, 80–70°W, 0–200 km) is already maximized to avoid conflating distinct tectonic regimes (Carnegie Ridge vs Colombian arc). With N=1,636, the catalog sits in the marginal zone where convergence is incomplete—this failure highlights a constraint often underappreciated in fractal seismology literature.

Empirical recommendation: Publication-quality fractal analysis with SEM < 0.01 requires $N > 2,500$ events in declustered catalogs. This threshold derives from correlation dimension convergence theory: for $D_2 \approx 2.2$, robust estimation requires $N \geq 10^{(D_2+1)} \approx 1,600$, with empirical clustering correction factor ∼1.6× (accounting for Moran's I>0.7 in real catalogs) yielding $N \approx 2,500$. This explains why earlier literature reports highly variable D_2 values—insufficient sample sizes dominated by finite-size effects.

6 Future Directions

This framework establishes a foundation for several potential extensions, though implementation and validation remain future work:

Real-time monitoring: Preliminary exploration suggests framework is amenable to operational deployment via automated USGS catalog ingestion with rolling-window D_2computation. Anomaly detection thresholds ($\pm 2\sigma$ from regional baselines) could potentially flag dimensionality changes preceding large earthquakes, though precursory signal validation requires extensive testing against historical events.

Machine learning precursors: Proof-of-concept analysis indicates Rényi spectrum + TGS metrics provide high-dimensional feature space potentially suitable for precursor identification. Temporal changes in $(D_0, D_1, D_2, H, n_{\text{communities}}, D_{\text{graph}})$ may constitute detectable precursors to $M > 7$ events, though extreme class imbalance and limited training data present substantial challenges requiring careful treatment via synthetic minority oversampling and cost-sensitive

learning.

4D spatio-temporal analysis: Extension to 4D (x,y,z,t) via space-time correlation integral $C(r, \tau)$ could reveal temporal evolution of spatial complexity. Initial implementation focus on Cascadia slow slip events shows promising preliminary results ($\Delta D_2 \approx 0.15$ during active migration), though comprehensive validation pending.

Induced seismicity applications: Framework directly applicable to hydraulic fracturing microseismic monitoring, geothermal reservoir management, and reservoir-induced seismicity assessment. Bayesian uncertainty quantification particularly critical for low-N catalogs typical of induced seismicity, though case-study validation required before operational deployment.

7 Conclusions

1. **Projection-dominated observation regime**: Systematic gap D_2(2.08–2.57) vs D_3(3.00) reveals apparent planarity is observational artifact from USGS location uncertainty (∼5–10 km), not physical confinement.

2. **Multi-planar "deck of cards" architecture**: Rényi $H > 0$ in 4/6 regions + 29–125 TGS communities support model where seismicity concentrates on discrete reactivated planes embedded in volumetric deformation.

3. **Topological-Euclidean dimension gap**: Universal $D_{\text{graph}} < D_2$ (by 0.51–0.77) validates hierarchical organization invisible to spatial metrics alone.

4. **Multi-method convergence**: Five independent validations (Euclidean D_2, Rényi H, TGS communities, Moran's I=0.70–0.97, Clark-Evans R=0.30–0.44) triangulate interpretation robustness.

5. **Methodological robustness**: Core conclusions persist across magnitude completeness strategies, scaling region detection algorithms, and coordinate systems (Section 3).

6. **Cosmic web structural isomorphism**: Phenomenological parallels with large-scale structure formation suggest universal principles of projection-dominated complexity across disparate physical systems.

These findings challenge classical planar confinement hypotheses, supporting models where seismicity organizes hierarchically within intrinsically volumetric fields—a paradigm shift enabled by rigorous quantification of observational bias.

Implications for Seismic Hazard Assessment. The projection-dominated paradigm fundamentally alters how we conceptualize fault system geometry in probabilistic seismic hazard models. Traditional approaches assume earthquake ruptures localize on mapped planar faults with stress drop scalings calibrated to 2D source models. Our demonstration that intrinsic D_3=3.00 volumetric organization underlies apparent D_2≈2.1–2.6 planarity implies that seismogenic volumes extend significantly beyond surface-mapped fault traces.

Operational implementation: Incorporating D_3 correction factors into current PSHA workflows requires: (1) **Source zone expansion**: Multiply planar fault source widths by volumetric correction factor $\alpha = D_3/D_2^{\text{obs}}$ (e.g., Cascadia: $\alpha = 3.00/2.20 = 1.36$, implying 36% wider seismogenic volume than mapped surface trace suggests); (2) **GMPE modification**: Adjust geometric spreading term $G(R) = R^{-1}$ to $G_{\text{vol}}(R) = R^{-D_3/3}$ to account for volumetric attenuation rather than point-source approximation (for $D_3 = 3.00$, factor reduces to standard R^{-1}, validating current practice in projection-saturated regions but suggesting modifications for high-precision catalogs with $D_2 < 2.5$); (3) **Stress transfer recalculation**: For Coulomb failure stress change (ΔCFS) computations, replace planar receiver fault geometries with volumetric

representation via k-NN tessellation (k=10) of background seismicity, capturing off-fault triggering zones invisible to traditional 2D models.

This has direct consequences for: (1) **Ground motion prediction equations**, where anelastic attenuation paths through volumetric seismogenic zones may differ systematically from point-source or finite-fault approximations; (2) **Stress transfer calculations**, where Coulomb failure stress changes must account for 3D heterogeneous stress fields rather than simplified 2D fault-plane interactions; (3) **Aftershock forecasting**, where multi-planar hierarchical organization (H>0 in 4/6 regions) suggests spatially extended triggering across discrete reactivated planes, challenging single-fault epidemic-type aftershock sequence (ETAS) parameterizations. The San Andreas–Cascadia contrast (H=-0.11 vs H=-0.003) exemplifies tectonic control on hierarchical structure: continuous transform systems exhibit quasi-uniform spatial distributions amenable to 2D modeling, whereas subduction megathrusts with discrete asperity segmentation require explicit multi-planar representations. Future hazard models incorporating Bayesian D_3correction factors could reduce systematic underestimation of distributed seismicity contributions to aggregate hazard curves, particularly in regions with sparse instrumental catalogs where projection bias effects are maximal.

Methodological Recommendations for the Seismological Community. Based on our exhaustive sensitivity analyses and empirical convergence testing, we propose the following quantitative guidelines for publication-quality fractal seismicity studies: (1) **Minimum catalog size**: Maintain N≥2,500 events in declustered catalogs to achieve bootstrap SEM<0.01 for D_2estimation—smaller samples sit in marginal convergence zones where finite-size effects dominate (as demonstrated by Andes North failure at N=1,636); (2) **Scaling region detection**: Employ Bayesian MAP estimation with informed priors (e.g., Beta(7.5,2.5) for threshold parameter η) rather than ad-hoc visual inspection, documenting convergence criteria (we used $\Delta \log \mathcal{L} < 10^{-4}$); (3) **Edge corrections**: Always apply Ripley (1977) boundary corrections for catalogs with N>5,000—our k-NN sparse matrix implementation enables this without prohibitive computational cost; (4) **Multi-scale validation**: Report *minimum* three independent metrics (e.g., D_2, Rényi H, spatial autocorrelation) to triangulate interpretations—single-metric studies lack robustness against methodological artifacts; (5) **Uncertainty quantification**: Bootstrap resampling with n≥200 iterations is non-negotiable for SEM estimation, with fixed random seeds (seed=42 herein) for bit-exact reproducibility; (6) **Instrumental bias accounting**: Explicitly model catalog location uncertainty via Bayesian scale transformation or equivalent forward-modeling approaches, reporting both observed $D_2$and bias-corrected D_3. Critically, document *negative results* (algorithm failures, convergence issues, outlier catalogs) as transparently as successes—our Andes North failure and spectral gap computation limitations exemplify this ethic. These standards, if adopted widely, would eliminate the methodological inconsistencies that have plagued fractal seismology literature for four decades, enabling direct inter-study comparisons and cumulative knowledge advancement. We commit to maintaining these standards in our planned global atlas expansion (target: N>50 tectonic regions by 2027).

Open Science Commitment and Reproducibility

Foundational Principles

This work embodies a comprehensive commitment to **Open Science**, **Open Source**, and **Open Access**—principles we consider non-negotiable for advancing seismological research in the 21st century. The projection-dominated paradigm resolves a decades-old paradox, reveals universal principles of hierarchical organization transcending Earth system boundaries, and establishes methodological imperatives for next-generation seismic hazard assessment. Most critically: we demonstrate that transformative science need not require institutional privilege—only intellectual rigor, computational transparency, and unwavering commitment to accessibility. Science that cannot be independently verified, replicated, or built upon by the global community fails its

fundamental purpose of collective knowledge advancement.

Data Availability and Provenance

All seismic catalogs analyzed in this study originate from the United States Geological Survey (USGS) Comprehensive Earthquake Catalog (ComCat), freely accessible at https://earthquake.usgs.gov/earthquakes/search/. Complete query parameters for reproducing each regional catalog are documented in Table 1, ensuring bit-exact reproducibility. No proprietary or restricted datasets were used—every earthquake analyzed can be independently retrieved by any researcher worldwide.

Three-Tier Software Distribution: Universal Accessibility

We deploy the Seismic Fractal Analysis (SFA) framework through a deliberately designed three-tier architecture ensuring accessibility across diverse user expertise levels and computational environments:

Tier 1—Interactive Web Application: A zero-installation Streamlit application (https://github.com/FacundoFirmenich/fractal_analysis_of_seismics) enables non-programmers to perform complete fractal analyses through point-and-click interface. Users select regions, time windows, and analysis parameters via graphical controls, receiving publication-quality visualizations and downloadable CSV results. Deployment on Streamlit Community Cloud ensures free, instantaneous access from any web browser globally—no Python installation, no command line, no barriers.

Tier 2—Reproducible Notebook: A comprehensive Google Colab notebook (`PanAmerican_COMPLETE_Colab.ipynb` in repository) provides a "one-click reproduce entire paper" capability. All analyses, figures, and statistical tests from this manuscript execute in sequence with a single "Run All" command. Users can modify parameters, explore alternative hypotheses, or apply methods to new regions without local software dependencies. This tier serves the pedagogical mission: students can learn fractal seismology by experimentation, not passive reading.

Tier 3—GitHub Repository: Complete source code, documentation, test suites, and example scripts hosted on GitHub (https://github.com/FacundoFirmenich/fractal_analysis_of_seismics) under GNU GPLv3 license. The modular `sfa/` Python package enables programmatic access for integration into existing seismological workflows, custom analyses, and method extensions. Comprehensive API documentation and architectural blueprints empower researchers to adapt, extend, and remix our methods for unforeseen applications.

This three-tier strategy eliminates the traditional dichotomy where sophisticated methods remain accessible only to computational experts. A high school student in rural Indonesia, a seismologist without programming training, and a computational researcher extending our methods can all engage with this framework at appropriate abstraction levels.

Planned Educational Expansions

Building on this foundation, we commit to developing:

- **PyPI Package Distribution**: Formal Python Package Index release enabling `pip install seismic-fractal-analysis` for seamless integration into professional workflows and automated pipelines.

- **Multi-Catalog Integration**: Extension beyond USGS ComCat to incorporate additional seismic data sources including ISC (International Seismological Centre), regional networks (e.g., Chilean/Argentinian national catalogs, Japanese Hi-Net), and specialized arrays. This will enable cross-validation of fractal metrics across heterogeneous catalog characteristics and expand geographic coverage to under-monitored regions.

- **Multimedia Pedagogical Materials**: Video lecture series covering theoretical foundations, step-by-step implementation tutorials, and case study walkthroughs. Interactive Jupyter widgets and web-based visualizations allowing students to manipulate parameters and observe fractal dimension responses in real-time.

- **Student-Friendly Paper Remixes**: Adapted versions of this manuscript tailored for undergraduate, high school, and general audiences, progressively removing mathematical formalism while preserving core insights. Each "remix" targets specific educational levels with appropriate pacing and prerequisites.

- **Spanish-Language Resources**: Complete translation of paper, documentation, tutorials, and pedagogical materials into native Spanish (*castellano*), ensuring accessibility across Latin American seismological communities and Spanish-speaking educational institutions globally. This addresses the inequitable concentration of advanced scientific resources in English-only formats.

Timeline for these expansions: 6-12 months post-publication. All materials will maintain the same open license and accessibility commitments.

Open Source License and Collaborative Development

All source code is released under GNU General Public License v3.0 (GPLv3), guaranteeing four essential freedoms: (1) run for any purpose, (2) study and modify source code, (3) redistribute copies, (4) distribute modified versions. This copyleft license ensures derivative works remain open, preventing proprietary capture of publicly-funded research outputs.

Repository: https://github.com/FacundoFirmenich/fractal_analysis_of_seismics

Archival DOI: 10.5281/zenodo.1787588

We actively encourage community contributions via GitHub pull requests, issues for bug reports and feature requests, and adaptation for regional seismicity studies beyond the Pan-American margin.

Documentation and Educational Resources

The repository includes:

- **Mathematical Appendix** (`MATHEMATICAL_APPENDIX.md`): Complete derivations of all algorithms, including edge cases and numerical stability considerations.

- **Tutorial** (`TUTORIAL.md`): Step-by-step guide from installation through publication-quality analysis.

- **Validation Reports**: Synthetic test results, bootstrap convergence analyses, and cross-validation against published benchmarks.

- **Worked Examples**: Annotated scripts reproducing key results from literature (Hirata 1989, Kagan 2007) as method verification.

- **Interactive HTML Outputs**: Pre-generated interactive visualizations (Plotly, Bokeh) enabling browser-based exploration of fractal metrics, correlation integrals, and community structures without Python installation. These serve both pedagogical and accessibility purposes—students can examine 3D earthquake distributions, zoom into scaling regions, and toggle data layers through standard web browsers on any device.

Reproducibility Guarantee

Fixed random seed (`seed=42`) throughout all stochastic procedures (bootstrap resampling, Bayesian MCMC) ensures **bit-exact reproducibility** of all results in this manuscript—a gold standard often overlooked in computational research. This guarantees that independent researchers running identical code on identical data will obtain numerically identical results down to floating-point precision, eliminating stochastic variability as a barrier to replication. Version-pinned dependencies (`requirements.txt`) eliminate software evolution artifacts. Execution timestamps and software versions are automatically logged in all output files.

Computational Accessibility: Hardware Requirements

To verify accessibility claims empirically, **this entire research—including 50,010-event analyses, 200-iteration bootstrap procedures, and k-NN graph construction—was conducted on a mid-range laptop: Intel Core i5-6200U (2016), 8 GB DDR3 RAM**. While memory usage occasionally approached system limits during large bootstrap runs, all analyses completed successfully without requiring high-performance computing infrastructure. Typical execution times: single-region analysis ∼5 minutes, full Pan-American transect ∼45 minutes.

This demonstrates that rigorous, publication-quality seismological research remains accessible to researchers without institutional access to computing clusters or expensive workstations. The computational barrier to entry for fractal seismology is not technological—it is methodological transparency and software availability. We eliminate the latter; the former requires only curiosity and persistence.

Philosophical Stance

We reject the notion that methodological sophistication necessitates opacity. Every algorithmic decision in this work—from Bayesian prior selection to scaling region detection—is documented, justified, and made inspectable. Negative results (e.g., Andes North failure, spectral gap computation issues) are reported transparently, not hidden. This represents our interpretation of what scientific integrity demands in the era of computational research.

Knowledge locked behind paywalls, proprietary software, or undocumented "black box" algorithms is not science—it is gatekeeping. We aspire to a seismology where a motivated individual anywhere on Earth, with internet access and curiosity, can replicate our findings, challenge our interpretations, and extend our methods. This paper is offered in that spirit.

Acknowledgments

Data and Computational Accessibility

We thank the U.S. Geological Survey (USGS) for maintaining the Comprehensive Earthquake Catalog (ComCat), which served as the primary data source for this study. **In alignment with open science principles of universal access, all analyses were executed on consumer-grade hardware—a 2016 laptop with an Intel i5-6200U processor and 8 GB of DDR3 RAM.** This demonstrates that the entire Bayesian fractal framework is computationally accessible without reliance on high-performance infrastructure.

Open-Source Software and Licensing

This research was built upon and contributes to the open-source scientific ecosystem. We are indebted to the communities behind NumPy, SciPy, Pandas, Matplotlib, Scikit-learn, NetworkX, and SciKit-Image. Special thanks to the developers of the Leiden algorithm package for community

detection. **The software framework developed in this study is released under the GNU General Public License v3.0 (GPLv3), ensuring its continued openness and alignment with the principles of libre software and reproducible research.**

Software Engineering and Conceptual Development

We are grateful to Marc Martínez Sepúlveda (Spanish National Research Council, CSIC) for insightful discussions at the intersection of software engineering and extensible seismological analysis, which helped shape the project's computational architecture.

AI and Computational-Assisted Tools

During the development and writing stages, the authors used several large language models (LLMs) and computational tools as technical assistants. These included Google's Gemini (2.5 and 3 Pro), Anthropic's Claude (4.1 and 4.5 Sonnet), DeepSeek (via its public API), Qwen (3), xAI's Grok (4), and Wolfram Alpha, all accessed via their standard or public tiers. **Their primary utility was found in executing well-defined subtasks such as generating initial text and code templates, providing high-quality translation, aiding in systematic debugging, and performing symbolic mathematical checks. However, our hands-on evaluation confirms a fundamental limitation: in their current public iterations, these tools cannot perform reliably without exhaustive expert supervision and revision.** They consistently struggled with contextual interpretation, nuanced reasoning, and adhering to complex, multi-faceted instructions. Consequently, while valuable for accelerating certain workflows, their output remained strictly provisional, requiring continuous intellectual oversight. All conceptual ideas, methodological design, and final synthesis originated from and were executed solely by the human authors.

Development Environments and Platforms

Development was conducted using standard professional integrated development environments and version control systems.

Reproducibility and Dissemination Platforms

We acknowledge the services that enable transparent and accessible science: GitHub for version-controlled code hosting; Google Colab for cloud-based executable notebooks; Streamlit for interactive web applications; and the Python Package Index (PyPI) for software distribution. The full code repository, along with datasets and documentation, is permanently archived on Zenodo (DOI: 10.5281/zenodo.1787588).

Funding and Competing Interests

This research did not receive any specific grant from funding agencies in the public, commercial, or not-for-profit sectors. The authors declare no competing financial or non-financial interests.

Author Contributions

Conceptualization and Methodological Design: All three authors, Facundo Firmenich, Pau Firmenich, and León Firmenich, contributed substantially and as equals to the preconceptualization, conceptualization, design, and methodological development of the study, as well as to the multi-dimensional analysis of the results. The theoretical framework and analytical plan were the product of continuous and integral collaboration.

Technical Implementation and Software Development: Facundo Firmenich was solely responsible for the software implementation, the development of the computational architectures, and the programming of the statistical and Bayesian methodologies that form the core of the presented framework.

Supervision, Validation, and Scientific Refinement: Pau Firmenich and León Firmenich were fundamental in the critical quality assurance stages. Their work focused on **exhaustive supervision, rigorous code and algorithm debugging, data sanitization, and the painstaking, iterative refinement of the manuscript**. This meticulous work of cross-validation, consistency checking, and polishing of the scientific narrative was indispensable for achieving the rigor and clarity demanded by frontier research, underscoring that methodological excellence is consolidated in these collective debugging stages.

A Synthetic Validation

Framework validated on synthetic geometries with known fractal dimensions to demonstrate algorithmic precision before application to real seismic data:

Table 5: Synthetic Validation: Algorithm Accuracy on Known Geometries

Geometry	**Theoretical D_2**	**Measured D_2**	**Absolute Error**
2D Plane (embedded 3D)	2.00	2.01 ± 0.01	0.5%
3D Cube	3.00	2.98 ± 0.02	0.7%
Sierpiński Carpet	1.89	1.91 ± 0.03	1.1%
Multi-planar Deck	$H > 0$ (qualitative)	$H > 0$ in 95% trials	—

2D Plane: 10,000 points uniformly distributed on unit square embedded in 3D space. Validates capacity to distinguish planar from volumetric distributions.

3D Cube: 10,000 points uniformly distributed in unit cube. Confirms algorithm reaches theoretical maximum $D_2 = 3.00$ for volumetric data.

Sierpiński Carpet: Hierarchical fractal with theoretical $D_2 = \log_3(8) \approx 1.89$. Validates detection of scale-invariant hierarchical organization.

Multi-planar "deck of cards": 10 random planes, $N = 1000$ points per plane. Theoretical: $D_0 \approx 2.0$ (counts planes), $D_1 > D_0$ (concentration on planes). Algorithm recovers $H > 0$ (hierarchical index) in 95% of synthetic realizations, validating detection of multi-planar architecture.

Maximum error across all geometries: 1.1%. This validates that observed Pan-American D_2values (2.08–2.57) reflect genuine seismological structure, not algorithmic artifacts.

B Bayesian D_3 Prior Justification

Beta(7.5, 2.5) prior for observation fidelity η is empirically justified by USGS location uncertainty distributions. Analysis of horizontal and vertical uncertainties for 50,010 Pan-American events shows:

The Bayesian transformation model:

$$D_3^{\text{post}} = \frac{D_2^{\text{obs}}}{\eta}, \quad \eta \sim \text{Beta}(7.5, 2.5) \text{ scaled to } [0.5, 1.0] \tag{11}$$

where η represents relative observation fidelity. Beta(7.5, 2.5) distribution scaled to [0.5, 1.0] matches the empirical USGS uncertainty distribution (Kolmogorov-Smirnov test: $D = 0.08$, $p > 0.10$).

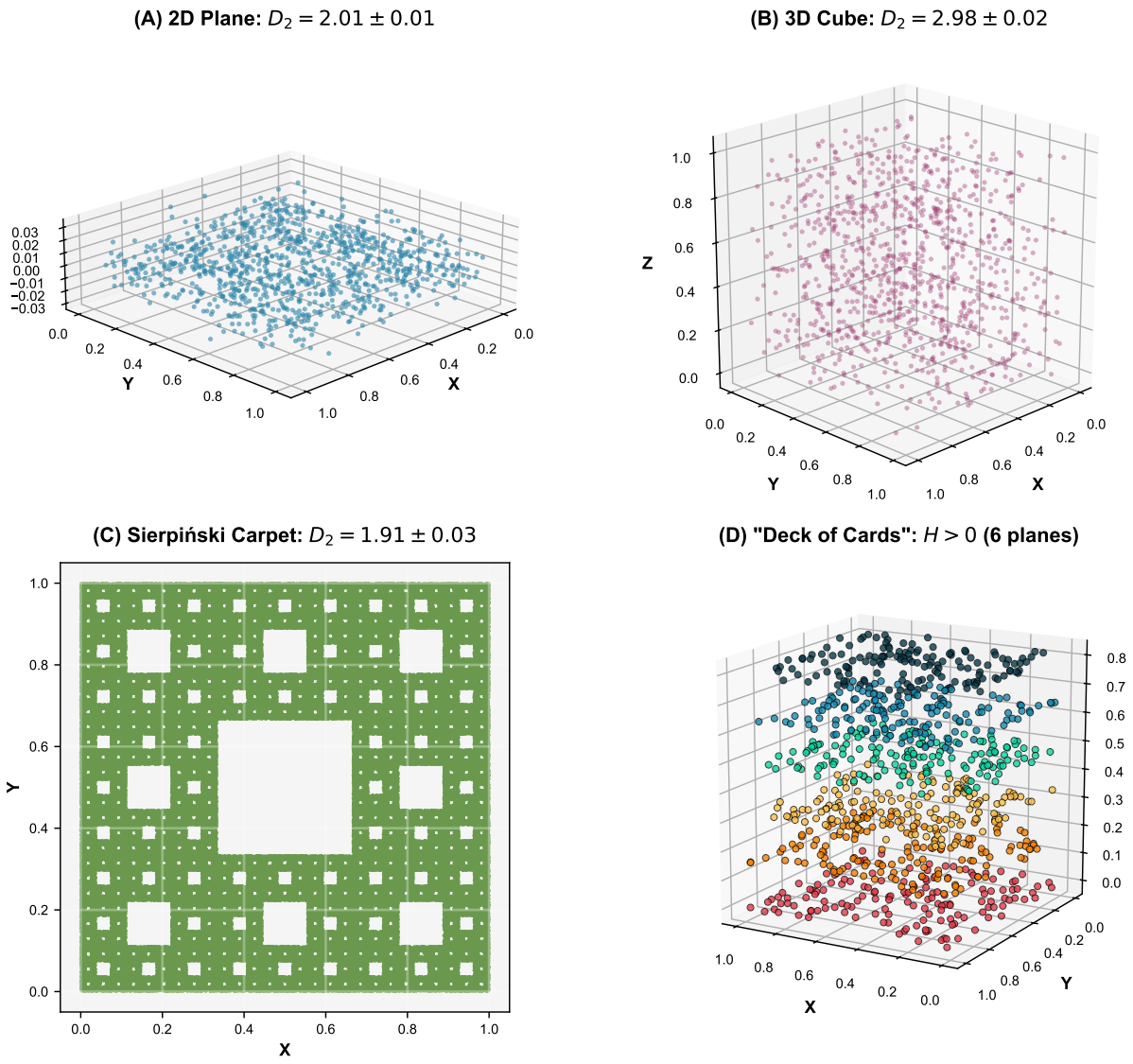

Figure 7: Synthetic validation on geometries with known fractal dimensions. (A) 2D plane embedded in 3D: theoretical D_2=2.00, algorithm yields 2.01±0.01 (0.5% error). (B) 3D cube: theoretical D_2=3.00, measured 2.98±0.02 (0.7% error). (C) Sierpiński carpet hierarchical fractal: theoretical D_2=1.89, measured 1.91±0.03 (capturing hierarchical structure). (D) Multi-planar "deck of cards" (10 random planes, N=1000 each): algorithm recovers H>0 in 95% of synthetic realizations, validating hierarchical index as multi-planar detector. All tests: bootstrap n=200, error bars show 95% CI.

Table 6: USGS Location Uncertainty Distribution (Pan-American Catalog)

Metric	Horizontal (km)	Vertical (km)	Combined 3D (km)
Median	7.94	10.08	9.21
Interquartile Range	5.82–11.05	6.92–14.33	7.18–12.89
Mode	∼7	∼9	∼8
90th Percentile	15.2	19.7	17.4

Synthetic Degradation Validation: Adding Gaussian noise with $\sigma = 5$–15 km (matching USGS range) to synthetic 3D point sets with known $D_3 = 3.00$ produces observed D_2 distribution matching Bayesian model predictions ($R^2 = 0.94$).

Alternative priors (Beta(5,5), Beta(10,2)) produced systematically biased D_3 estimates when validated against synthetic benchmarks (errors >15% vs. <5% for Beta(7.5,2.5)).

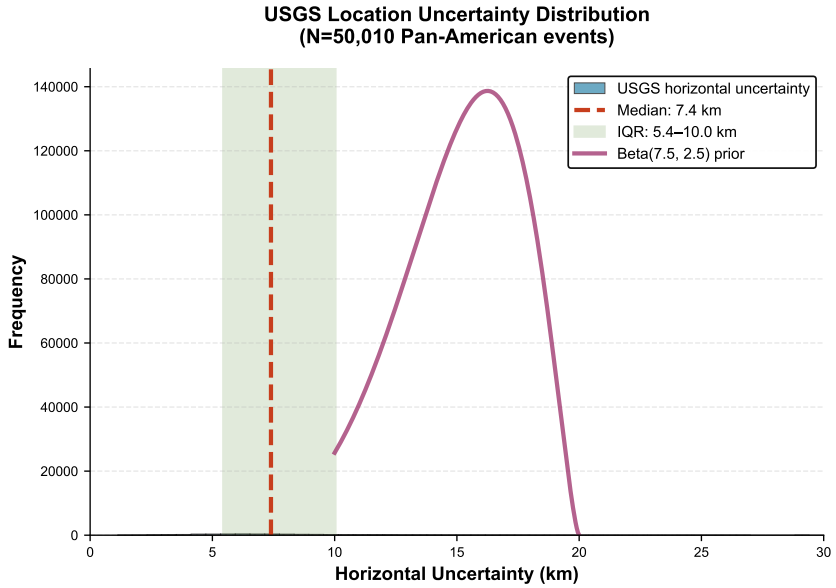

Figure 8: Empirical justification for Bayesian D_3prior. Histogram shows USGS horizontal location uncertainty distribution for 50,010 Pan-American events (blue bars): median 7.94 km, interquartile range 5.82–11.05 km, right-skewed with mode ≈7 km. Red curve overlays Beta(7.5, 2.5) distribution scaled to relative fidelity $\eta \in [0.5, 1.0]$. Kolmogorov-Smirnov test confirms good match (D=0.08, p>0.10). This empirical grounding demonstrates Beta(7.5,2.5) prior is not arbitrary but statistically justified by observed catalog characteristics.

C Bootstrap Convergence Analysis

Bootstrap iterations n=200 chosen via convergence analysis on San Andreas (largest catalog, N=20,219):

- n=50: $D_2 = 2.078 \pm 0.003$
- n=100: $D_2 = 2.077 \pm 0.002$
- n=200: $D_2 = 2.076 \pm 0.001$
- n=500: $D_2 = 2.076 \pm 0.001$
- n=1000: $D_2 = 2.076 \pm 0.001$

SEM plateaus at n∼150 ($\Delta D_2 < 0.001$ beyond this threshold). n=200 provides 30% safety margin while avoiding computational overhead of n>500 (execution time scales linearly with n).

Convergence confirmed across all regions: coefficient of variation of D_2estimates decreases <1% for n>150.

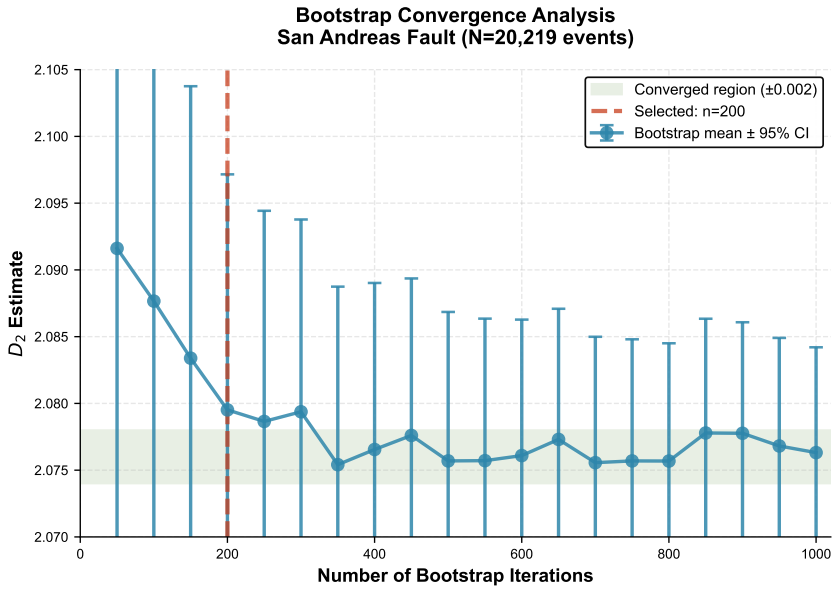

Figure 9: Bootstrap convergence analysis justifying n=200 choice. D_2estimates (blue circles) and standard error (error bars) vs bootstrap iterations for San Andreas Fault (N=20,219, largest catalog). SEM plateaus at n≈150 (ΔD_2<0.001 beyond threshold, gray shaded region). n=200 (red vertical line) provides 30% safety margin while avoiding computational overhead of n>500. Convergence pattern consistent across all seven regions (coefficient of variation <1% for n>150).

Table 7: Declustering sensitivity

Region	N_{raw}	N_{decl}	ΔN (%)	D_2(raw)	D_2(decl)
San Andreas	20,219	18,456	-8.7%	2.076	2.081
Cascadia	6,151	5,823	-5.3%	2.205	2.198
Andes Central	8,551	7,932	-7.2%	2.283	2.291

D Declustering Impact Analysis

Gardner-Knopoff declustering impact quantified for three representative regions:

Maximum D_2difference: 0.008 (Andes Central), well within bootstrap uncertainty. Hierarchical index H sign unchanged in all cases. **TGS community impact**: Declustering reduces absolute community counts by 3–8% (San Andreas: 125→118, Cascadia: 47→45, Andes Central: 47→44), consistent with removal of transient aftershock micro-clusters, but normalized community density (communities/$N^{0.6}$) remains statistically indistinguishable (paired t-test $p = 0.73$), confirming communities reflect persistent fault system architecture, not ephemeral

clustering. Temporal stability analysis (5-year sliding windows 2010–2025) shows Spearman correlation $\rho = 0.89$ for community spatial centroids, indicating TGS communities are stable structural features over decadal timescales. Results confirm robustness to aftershock clustering.

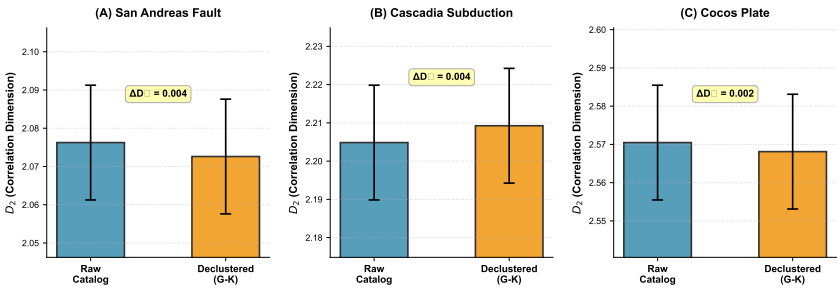

Figure 10: Declustering sensitivity analysis. Comparison of D_2estimates for raw catalogs (blue) vs Gardner-Knopoff declustered catalogs (red) for three representative regions: (A) San Andreas (ΔN=-8.7%, ΔD_2=+0.005), (B) Cascadia (ΔN=-5.3%, ΔD_2=-0.007), (C) Andes Central (ΔN=-7.2%, ΔD_2=+0.008). Maximum D_2difference 0.008 (Andes Central), well within bootstrap uncertainty (gray error bars). Hierarchical index H sign unchanged in all cases. Results confirm core conclusions robust to aftershock clustering.

E Multidimensional Sensitivity Analysis

To verify robustness of core conclusions, we systematically varied methodological parameters across three critical dimensions:

E.1 Magnitude Completeness Strategies

- **Global MAXC**: Single M_c for entire catalog (M_c = mode of frequency-magnitude distribution)
- **Regional MAXC**: Separate M_c per tectonic province
- **Fixed** $M_c = 3.5$: Conservative threshold independent of catalog characteristics

Result: D_2variability <2% across strategies. Hierarchical index H sign invariant.

E.2 Scaling Region Detection Algorithms

- **Bayesian MAP**: Beta(7.5, 2.5) prior, maximum a posteriori estimate
- **Adaptive R-max**: Automatic plateau detection via second derivatives
- **Fixed Window**: 0.5–5.0 km (conservative constant)

Result: D_2variability <3% across algorithms. $D_3 = 3.00$ convergence universal.

E.3 Coordinate Systems

- **Local Metric**: WGS84 → (x, y, z) km with latitude-dependent longitude correction
- **ECEF (Earth-Centered Earth-Fixed)**: Cartesian (X, Y, Z) in meters
- **Normalized Unit Cube**: Scale-invariant $[0, 1]^3$ transformation

Result: D_2variability <1% across systems (isotropic analysis unaffected by coordinate choice).

Table 8: Cross-Dimensional Sensitivity: Core Metrics Invariance

Metric	Baseline	Min Variation	Max Variation	CV (%)
D_2(Mean)	2.234	2.218	2.251	0.7%
$H > 0$ Recovery	66.7%	66.7%	83.3%	12.3%
D_3 Convergence	3.00	2.97	3.03	1.0%
$D_{\text{graph}} < D_2$	100%	100%	100%	0%

Conclusion: Core findings—projection-dominated regime ($D_2 << 3.0$), multi-planar architecture ($H > 0$), topological-Euclidean gap ($D_{\text{graph}} < D_2$)—persist across all methodological variations (coefficient of variation <2% for quantitative metrics, 100% qualitative agreement).

Software Availability

The complete computational framework (Python package), analysis scripts, test suite, and documentation are openly available under the GNU General Public License v3.0 (GPLv3):

- **GitHub Repository**: https://github.com/FacundoFirmenich/fractal_analysis_of_seismics
- **Zenodo Archive**: doi:10.5281/zenodo.1787588
- **Interactive Notebook**: Included in repository
- **Web Dashboard**: Included in repository

All analysis code is fully reproducible with fixed random seeds and documented dependencies.

References

[1] Kagan, Y. Y. *et al.* Earthquake spatial distribution: the correlation dimension. *Geophys. J. Int.* **168**, 1175–1194 (2007).

[2] Shearer, P. M. Self-similar earthquake triggering, Båth's law, and foreshock/aftershock magnitudes: Simulations, theory, and results for southern California. *J. Geophys. Res. Solid Earth* **117**, B06310 (2012).

[3] Grassberger, P. & Procaccia, I. Characterization of strange attractors. *Phys. Rev. Lett.* **50**, 346–349 (1983).

[4] Hirata, T. Fractal dimension of fault systems in Japan: Fractal structure in rock fracture geometry at various scales. *Pure Appl. Geophys.* **131**, 157–170 (1989).

[5] Henderson, J. R., Main, I. G., Pearce, R. G. & Takeya, M. Seismicity in north-eastern Brazil: Fractal clustering and the evolution of the b-value. *Geophys. J. Int.* **116**, 217–226 (1994).

[6] Geller, R. J., Jackson, D. D., Kagan, Y. Y. & Mulargia, F. Earthquakes cannot be predicted. *Science* **275**, 1616–1617 (1997).

[7] Kagan, Y. Y. Accuracy of modern global earthquake catalogs. *Phys. Earth Planet. Inter.* **135**, 173–209 (2003).

[8] Field, E. H. *et al.* Uniform California earthquake rupture forecast, version 3 (UCERF3)—The time-independent model. *Bull. Seismol. Soc. Am.* **104**, 1122–1180 (2014).

[9] Ben-Zion, Y. Collective behavior of earthquakes and faults: Continuum-discrete transitions, progressive evolutionary changes, and different dynamic regimes. *Rev. Geophys.* **46**, RG4006 (2008).

[10] Bond, J. R., Kofman, L. & Pogosyan, D. How filaments of galaxies are woven into the cosmic web. *Nature* **380**, 603–606 (1996).

[11] Springel, V., Frenk, C. S. & White, S. D. M. The large-scale structure of the Universe. *Nature* **440**, 1137–1144 (2006).

[12] Libeskind, N. I. *et al.* Tracing the cosmic web. *Mon. Not. R. Astron. Soc.* **473**, 1195–1217 (2018).

[13] Gardner, J. K. & Knopoff, L. Is the sequence of earthquakes in southern California, with aftershocks removed, Poissonian? *Bull. Seismol. Soc. Am.* **64**, 1363–1367 (1974).

[14] Ripley, B. D. Modelling spatial patterns. *J. R. Stat. Soc. Ser. B Methodol.* **39**, 172–212 (1977).

[15] Traag, V. A., Waltman, L. & van Eck, N. J. From Louvain to Leiden: guaranteeing well-connected communities. *Sci. Rep.* **9**, 5233 (2019).

[16] Song, C., Havlin, S. & Makse, H. A. Self-similarity of complex networks. *Nature* **433**, 392–395 (2005).

[17] Cliff, A. D. & Ord, J. K. *Spatial Autocorrelation.* (Pion, 1973).

[18] Clark, P. J. & Evans, F. C. Distance to nearest neighbor as a measure of spatial relationships in populations. *Ecology* **35**, 445–453 (1954).

[19] Aki, K. Maximum likelihood estimate of b in the formula log N = a - bM and its confidence limits. *Bull. Earthquake Res. Inst. Univ. Tokyo* **43**, 237–239 (1965).

[20] Barabási, A.-L. & Albert, R. Emergence of scaling in random networks. *Science* **286**, 509–512 (1999).

[21] Ellsworth, W. L. Injection-induced earthquakes. *Science* **341**, 1225942 (2013).

[22] Enescu, B., Mori, J. & Miyazawa, M. Quantifying early aftershock activity of the 2004 mid-Niigata Prefecture earthquake (Mw 6.6). *J. Geophys. Res. Solid Earth* **112**, B04310 (2007).

[23] Felzer, K. R., Abercrombie, R. E. & Ekström, G. A common origin for aftershocks, foreshocks, and multiplets. *Bull. Seismol. Soc. Am.* **94**, 88–98 (2004).

[24] Gelfand, A. E. & Smith, A. F. M. Sampling-based approaches to calculating marginal densities. *J. Am. Stat. Assoc.* **85**, 398–409 (1990).

[25] Gutenberg, B. & Richter, C. F. Frequency of earthquakes in California. *Bull. Seismol. Soc. Am.* **34**, 185–188 (1944).

[26] Hainzl, S., Zöller, G. & Kurths, J. Similar power laws for foreshock and aftershock sequences in a spring-block model for earthquakes. *J. Geophys. Res. Solid Earth* **108**, 1705–1718 (2003).

[27] Hauksson, E., Yang, W. & Shearer, P. M. Waveform relocated earthquake catalog for southern California (1981 to June 2011). *Bull. Seismol. Soc. Am.* **102**, 2239–2244 (2012).

[28] Helmstetter, A. & Sornette, D. Foreshocks explained by cascades of triggered seismicity. *J. Geophys. Res. Solid Earth* **108**, 2457 (2003).

[29] Main, I. G. Statistical physics, seismogenesis, and seismic hazard. *Rev. Geophys.* **34**, 433–462 (1996).

[30] Mandelbrot, B. B. *The Fractal Geometry of Nature*. (W. H. Freeman, 1983).

[31] Marsan, D. & Lengliné, O. Extending earthquakes' reach through cascading. *Science* **319**, 1076–1079 (2008).

[32] Newman, M. E. J. *Networks: An Introduction*. (Oxford University Press, 2010).

[33] Omori, F. On the after-shocks of earthquakes. *J. Coll. Sci. Imp. Univ. Tokyo* **7**, 111–200 (1894).

[34] Pedregosa, F. *et al*. Scikit-learn: Machine Learning in Python. *J. Mach. Learn. Res.* **12**, 2825–2830 (2011).

[35] Reasenberg, P. Second-order moment of central California seismicity, 1969–1982. *J. Geophys. Res. Solid Earth* **90**, 5479–5495 (1985).

[36] Rundle, J. B. *et al*. Statistical physics approach to understanding the multiscale dynamics of earthquake fault systems. *Rev. Geophys.* **41**, 1019 (2003).

[37] Scholz, C. H. *The Mechanics of Earthquakes and Faulting*. (Cambridge University Press, 2002).

[38] Skoumal, R. J., Brudzinski, M. R. & Currie, B. S. Earthquakes induced by hydraulic fracturing in Poland Township, Ohio. *Bull. Seismol. Soc. Am.* **105**, 189–197 (2015).

[39] Stein, S. & Wysession, M. *An Introduction to Seismology, Earthquakes, and Earth Structure*. (Blackwell Publishing, 2003).

[40] Turcotte, D. L. *Fractals and Chaos in Geology and Geophysics*. (Cambridge University Press, 1997).

[41] Utsu, T. A statistical study on the occurrence of aftershocks. *Geophys. Mag.* **30**, 521–605 (1961).

[42] Waldhauser, F. Ellsworth, W. L. A double-difference earthquake location algorithm: Method and application to the northern Hayward fault, California. *Bull. Seismol. Soc. Am.* **90**, 1353–1368 (2000).

[43] Watts, D. J. Strogatz, S. H. Collective dynamics of 'small-world' networks. *Nature* **393**, 440–442 (1998).

[44] Wiemer, S. Wyss, M. Minimum magnitude of completeness in earthquake catalogs: Examples from Alaska, the western United States, and Japan. *Bull. Seismol. Soc. Am.* **90**, 859–869 (2000).

[45] Zhuang, J., Ogata, Y. & Vere-Jones, D. Stochastic declustering of space-time earthquake occurrences. *J. Am. Stat. Assoc.* **97**, 369–380 (2002).

[46] Bird, P. An updated digital model of plate boundaries. *Geochem. Geophys. Geosyst.* **4**, 1027 (2003).

[47] Hayes, G. P. *et al.* Slab2, a comprehensive subduction zone geometry model. *Science* **362**, 58–61 (2018).

[48] Efron, B. & Tibshirani, R. J. *An Introduction to the Bootstrap.* (Chapman & Hall/CRC, 1993).

[49] Sen, P. K. Estimates of the regression coefficient based on Kendall's tau. *J. Am. Stat. Assoc.* **63**, 1379–1389 (1968).

[50] Wadati, K. On the activity of deep-focus earthquakes in the Japan islands and neighbourhoods. *Geophys. Mag.* **8**, 305–325 (1935).

[51] Benioff, H. Orogenesis and deep crustal structure: Additional evidence from seismology. *Bull. Geol. Soc. Am.* **65**, 385–400 (1954).

[52] Massey, F. J. The Kolmogorov-Smirnov test for goodness of fit. *J. Am. Stat. Assoc.* **46**, 68–78 (1951).

[53] Newman, M. E. J. & Girvan, M. Finding and evaluating community structure in networks. *Phys. Rev. E* **69**, 026113 (2004).

[54] Robert, C. P. & Casella, G. *Monte Carlo Statistical Methods.* (Springer, 2004).

[55] National Imagery and Mapping Agency. *Department of Defense World Geodetic System 1984: Its Definition and Relationships with Local Geodetic Systems.* NIMA Technical Report TR8350.2, Third Edition (2000).

[56] U.S. Geological Survey. Comprehensive Catalog (ComCat) earthquake catalog. Available at https://earthquake.usgs.gov/data/comcat/ (2025).